Electronic Supplementary Information for

Crystal Phase Transformation of Tungsten Oxide: A Novel Route to Oxygen Vacancy Engineering for Highly Active Epoxidation Catalysts

Baoliang Lv,[#,a,b] Duojia Ren,[#,a] Qi Zhang,[b,c] Wei Zhang,[a] Miao Zhang,[a] Xining Yang,[d] Shoufeng Xue,[a] Wenting Lv[a,b] and Huixiang Wang[,a, b]*

[a]School of Chemistry and Chemical Engineering, Shanxi Normal University, Taiyuan 030031, China. E-mail: lvbl@sxnu.edu.cn; wanghx@sxnu.edu.cn

[b]Shanxi Key Laboratory of Coal-based Synthetic Oil Product Testing, Changzhi 046000, China.

[c]Changzhi Comprehensive Inspection and Testing Center, Changzhi 046000, China.

[d]School of Resources and Environmental Science, Hubei University, Wuhan 430062, China.

#: These authors contributed equally.

Experimental section

Materials and reagents

All chemical reagents were used as received without any further purification. Tungsten chloride (WCl_6, 99%), acetonitrile (MeCN, 99%), anisole (C_7H_8O, 99%), ethylacetate ($C_4H_8O_2$, 99%), cyclooctene (C_8H_{14}, 95%), 1-hexene (C_6H_{12}, 99%), 1-octene (C_8H_{16}, 98%), 1-decene ($C_{10}H_{20}$, 95%), 1-dodecene ($C_{12}H_{24}$, 95%), cis-stilbene ($C_{14}H_{12}$, 97%), cis-stilbene oxide ($C_{14}H_{12}O$, 95%) were purchased from Aladdin Co. Hydrogen peroxide (H_2O_2, 30 wt %) and anhydrous ethanol (EtOH, 99%) were purchased from Tianjin Chemical Reagent Co. Distilled water with a specific resistance of 18.2 MΩ·cm was used throughout the experiments.

Preparation method of catalyst:

The catalyst of $WO_3 \cdot H_2O/W_{18}O_{49}$ was prepared by a solvothermal method as follows: 1.570 g of WCl_6 was dissolved in 60 mL of anhydrous ethanol and magnetically stirred until complete dissolution, and the solution turned yellow. The solution was transferred to a 100 mL hydrothermal reactor and reacted at 140 °C for 2 h, 4 h, 6 h, 8 h, 10 h, 12 h, respectively. After cooling to room temperature, the product was washed three times with distilled water and ethanol, respectively, and dried at 60 °C for 5 h to obtain dark blue products, and the obtained catalysts were labeled as W2, W4, W6, W8, W10 and W12, specially, the sample obtained with 10 h reaction was also named $WH/WO_{2.72}$.

Physical measurements and instrumentation

The JSM-IT800 (SHL) SEM was employed for observing morphology, size, and nanoparticle distribution of catalysts. Crystal structure was analyzed using SmartLab XRD with Cu-Kα radiation (λ=1.54056 Å; 40 kV, 40 mA, 10° min^{-1}, 2θ = 10°–90°) and phases identified via PDF card matching. FEI Talos F200X G2 TEM/HRTEM measured lattice spacing of catalyst. Surface elemental composition and valence states

were determined by XPS (Thermo Scientific K-alpha+, Al-Kα), with binding energies referenced to C 1s (284.8 eV) and analyzed using Avantage software. Oxygen vacancies were detected via low-temperature EPR (Bruker EMXplus-6/1) at 100 K and above XPS technology. The Raman spectroscopy was recorded by RENISHAW with 532 nm excitation and 200-1200 cm^{-1} range.

Catalytic activity tests

The catalytic reaction was carried out in a 25 mL stainless steel autoclave. In the epoxidation reaction, 4 mmol cyclooctene, 4 mmol H_2O_2 (30 wt%) and 30 mg catalyst were dispersed in 10 ml acetonitrile. The suspension was then stirred at 600 r min^{-1} and under 60 ℃ for 4 h. Timing started when the temperature increased to the target temperature. After the reaction, anisole as internal standard was added and stirred, then the supernatant was taken after centrifugation and analyzed by gas chromatography (GC, GC-950) and Shimadzu gaschromatography-mass spectrometry (GC-MS, QP-2050).

Tab. S1. The proportion of $O_{ads.}$ and W^{5+}, and oxygen vacancy concentration in different samples based on XPS and EPR quantification.

Samples	$O_{ads.}$ and W^{5+} proportion (%)		oxygen vacancy concentration
	$O_{ads.}/(O_{lat.}+O_{ads.}+O_{-OH})$	$W^{5+}/(W^{5+}+W^{6+})$	spins/mg
W4	8.34	6.84	4.329×10^{16}
$WH/WO_{2.72}$	15.62	15.07	7.633×10^{16}
W12	18.10	17.22	8.340×10^{16}

Tab. S2. Specific surface area and pore information for different samples.

Samples	S_{BET} ($m^2\cdot g^{-1}$)	Pore volume ($cm^3\cdot g^{-1}$)	Average pore size (nm)
W4	27.25	0.104	15.26
W6	25.92	0.128	19.74
W8	38.47	0.124	12.92
W10($WH/WO_{2.72}$)	87.81	0.225	10.25
W10($WH/WO_{2.72}$) (after reaction)	82.35	0.203	9.96
W12	47.15	0.100	8.48

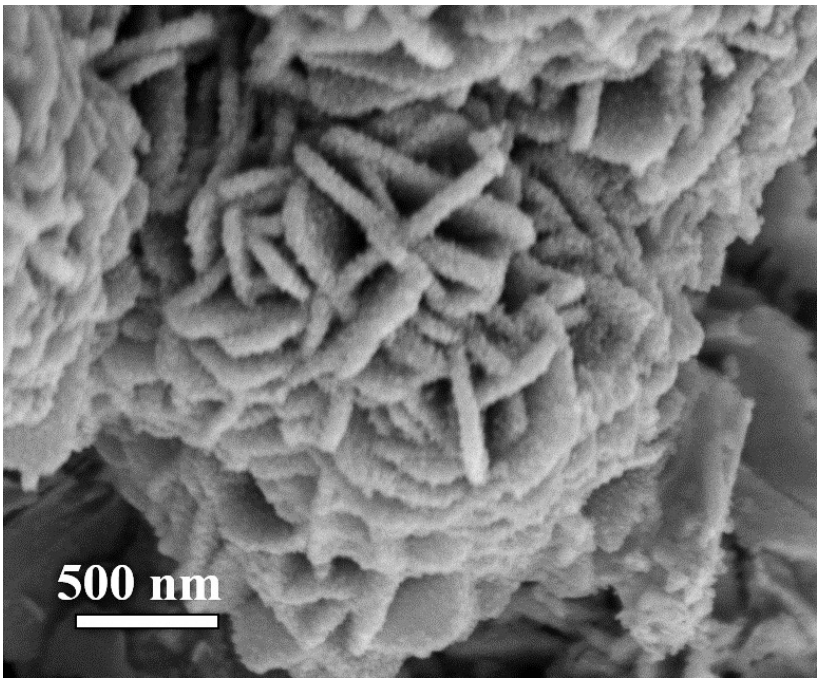

Fig. S1. SEM image of $WH/WO_{2.72}$ after five reaction cycles.

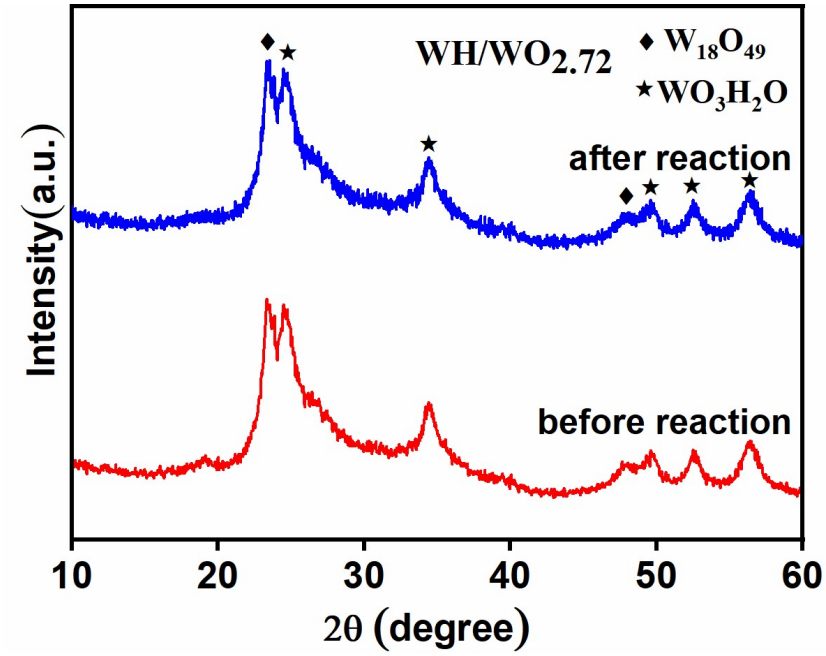

Fig. S2. XRD patterns of $WH/WO_{2.72}$ before and after five reaction cycles.

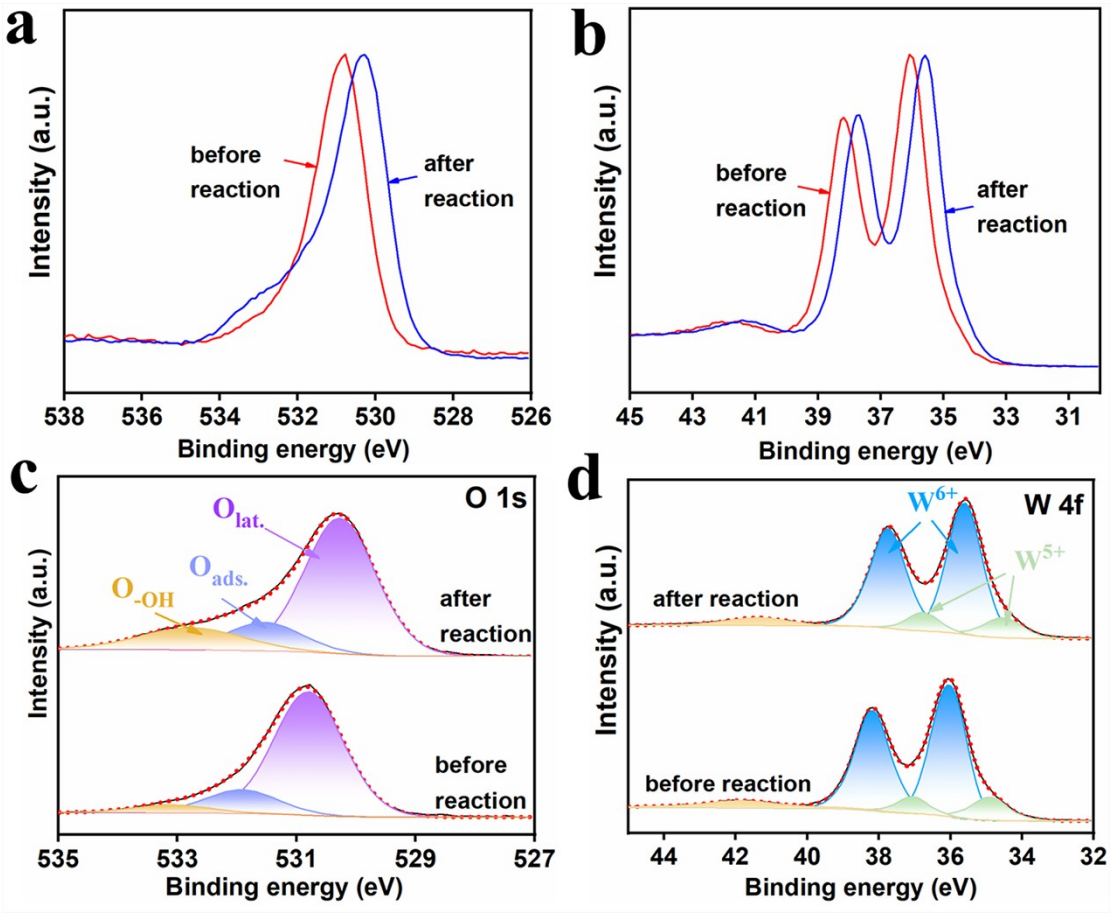

Fig. S3. XPS binding energy of O 1s (a, c) and W 4f (b, d) in $WH/WO_{2.72}$ before and after five reaction cycles.

Tab. S3. The proportion of $O_{ads.}$ and W^{5+}, and oxygen vacancy concentration in $WH/WO_{2.72}$ before and after five reaction cycles based on XPS and EPR quantification.

Samples	$O_{ads.}$ and W^{5+} proportion (%)		oxygen vacancy concentration
	$O_{ads.}/(O_{lat.}+O_{ads.}+O_{-OH})$	$W^{5+}/(W^{5+}+W^{6+})$	spins/mg
$WH/WO_{2.72}$	15.62	15.07	7.633×10^{16}
$WH/WO_{2.72}$ (after reaction)	15.06	14.08	7.021×10^{16}

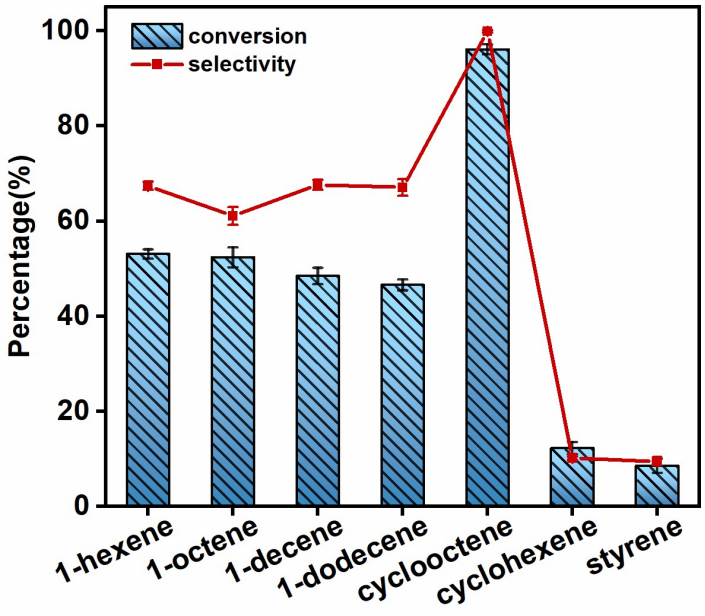

Fig. S4. Epoxidation activity of WH/$WO_{2.72}$ for different long chain α-olefins, cyclohexene and styrene.

It can be seen from the Fig. S4, WH/$WO_{2.72}$ exhibits the following activity and selectivity order: cyclooctene > long-chain α-olefins > cyclohexene > styrene. In olefin epoxidation, attack of electrophilic oxygen from the active intermediate species on the olefinic C=C bond is the key step of the reaction, and a higher electron density of the C=C bond favors the reaction. So the fundamental reason for the difference in conversion (activity) in these olefins lies in their distinct structures.

The eight-membered ring of cyclooctene exhibits a certain ring strain, and its C=C bond is fully exposed at the apex of the boat-chair conformation (Fig. S5) [1], making the C=C bond more vulnerable to electrophilic oxygen attack. Moreover, the C=C bond does not conjugate with the large ring, so the electron is concentrated on the C=C bond, leading to a specific attack site.

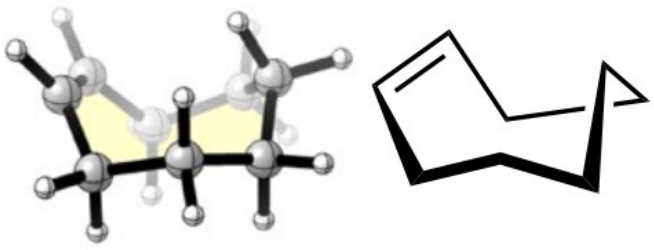

Fig. S5. The spatial structure of cyclooctene.

Long chain α-olefins have no ring strain; their C=C bonds only experience a weak electron-donating effect from alkyl groups, resulting in a moderate electron density of the C=C bond. In addition, the hydrophobic carbon chain tends to bend and wrap around the C=C bond, increasing the steric hindrance and thus lowering the reactivity. Furthermore, for heterogeneous catalysts such as transition metal oxides, a lot of hydrophilic -OH are usually present on their surfaces. The hydrophobic alkyl chains of long chain α-olefins generate a hydrophobic-hydrophilic repulsion with the hydrophilic catalyst surface, and this effect further reduces the probability of the electrophilic attack of active species on the catalyst surface towards the C=C bond.

The low reactivity of cyclohexene is mainly attributed to the high stability of its six-membered ring (low ring strain) and low electron density of the C=C bond due to its intrinsic property of internal alkene. For styrene, the low reactivity arises primarily from the π-π conjugation between the C=C bond and the benzene ring, which leads to the delocalization of the electron cloud toward the aromatic ring and thus reduces the electron density of the C=C bond.

As for selectivity, the three-membered epoxide ring of cyclooctene oxide is directly embedded in the eight-membered ring skeleton (inside the boat conformation), which creates large steric hindrance against ring-opening. Therefore, it is less prone to ring-opening hydrolysis and deep oxidation. By contrast, the three-membered epoxide ring of 1,2-long chain alkylene oxides is located at the terminal position, with slightly lower steric hindrance to ring-opening hydrolysis and subsequent deep oxidation (yielding 1,2-diol and acids with one bond cleaved), thus giving more by-products. The poor selectivity for both cyclohexene and styrene due to their low electron density of the C=C bond, making it a less favorable site for oxidation, which leads to more side reactions and consequently lower selectivity toward the epoxide product.

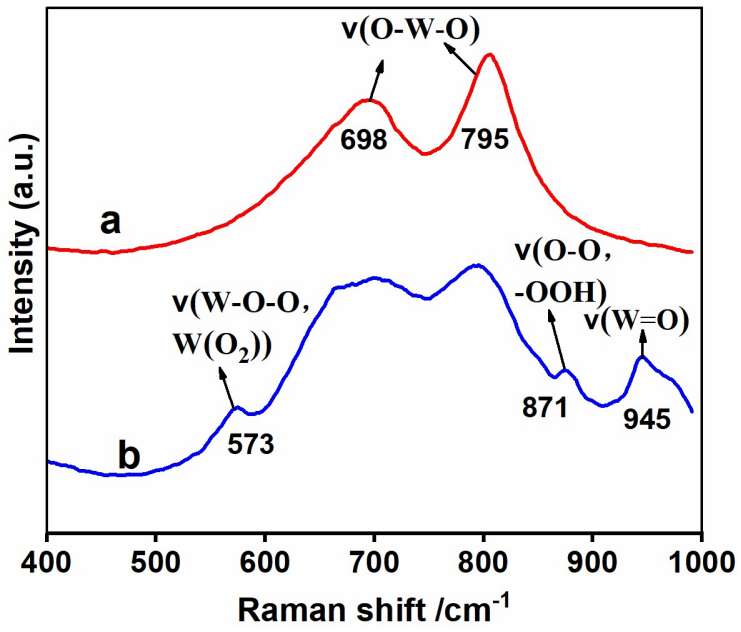

Fig. S6. Raman spectra of WH/$WO_{2.72}$ with (a) fresh catalyst and (b) after H_2O_2 treatment.

In the research field of WO_3-catalyzed epoxidation, there is a general consensus among researchers that the interaction of WO_3 and H_2O_2 can generate W-(η^2-O_2) or W-OOH species as active intermediate for epoxidation [2-7]. Raman spectroscopy can be used to detect the formation of peroxotungsten species. Fig. S6 presents the Raman spectra of WH/$WO_{2.72}$ before (a) and after (b) treatment with a trace amount of H_2O_2. It can be seen that three new peaks appear in the H_2O_2-treated sample. Consistent with literature reports, the band at 573 cm^{-1} is ascribed to the ν(W-O-O, $W(O_2)$), while the 871 cm^{-1} peak is assigned to either the ν(O-O) [3,8] or the ν(-OOH) [9-11], and the band at 945 cm^{-1} belongs to ν(W=O) [3, 12]. Therefore, according to the Raman results, both tungsten peroxide species of W-(η^2-O_2) and W-OOH may be generated. However, Raman spectra alone cannot determine which species acts as the dominant active intermediate, and further verification is required. Moreover, it is the emergence of the tungsten peroxo structures and terminal W=O bonds that disrupts the uniformity of the original O–W–O vibrational modes and makes them more complex, thus leading to peak broadening.

According to existing studies [13,6], the W-OOH follows a concerted oxidation mechanism in alkene epoxidation, which prevents stereochemical rearrangement. That is to say, if cis-stilbene is used as the substrate, the prominent product will be cis-stilbene oxide. In contrast, the W-(η^2-O_2) proceeds via a stepwise mechanism that does not inhibit stereochemical rearrangement, and when transferring the electrophilic oxygen atom to cis-stilbene, it generates cis- and trans-stilbene oxides in comparable concentrations. Based on this, we employed cis-stilbene as the reaction substrate for experimental verification.

Fig. S7 is the GC chromatogram for the epoxidation of cis-stilbene with H_2O_2 over $WH/WO_{2.72}$ catalyst, the reaction solvent is acetonitrile, and the extraction solvent is ethyl acetate. Products 1–8 identified by GC-MS (QP-2050) are also labeled in the figure. Among them, 2 and 6 correspond to cis- and trans-stilbene oxide, respectively. It is evident that the yield of the cis-product is much higher than that of the trans-product, indicating that the key intermediate is W–OOH. Accordingly, in line with previous reports, for $W_{18}O_{49}$, the sites for formation of W–OOH are also mainly ascribed to oxygen vacancies [6,7]. For $WO_3 \cdot H_2O$, the generation of W–OOH arises from the longer W–H_2O bond [14, 5].

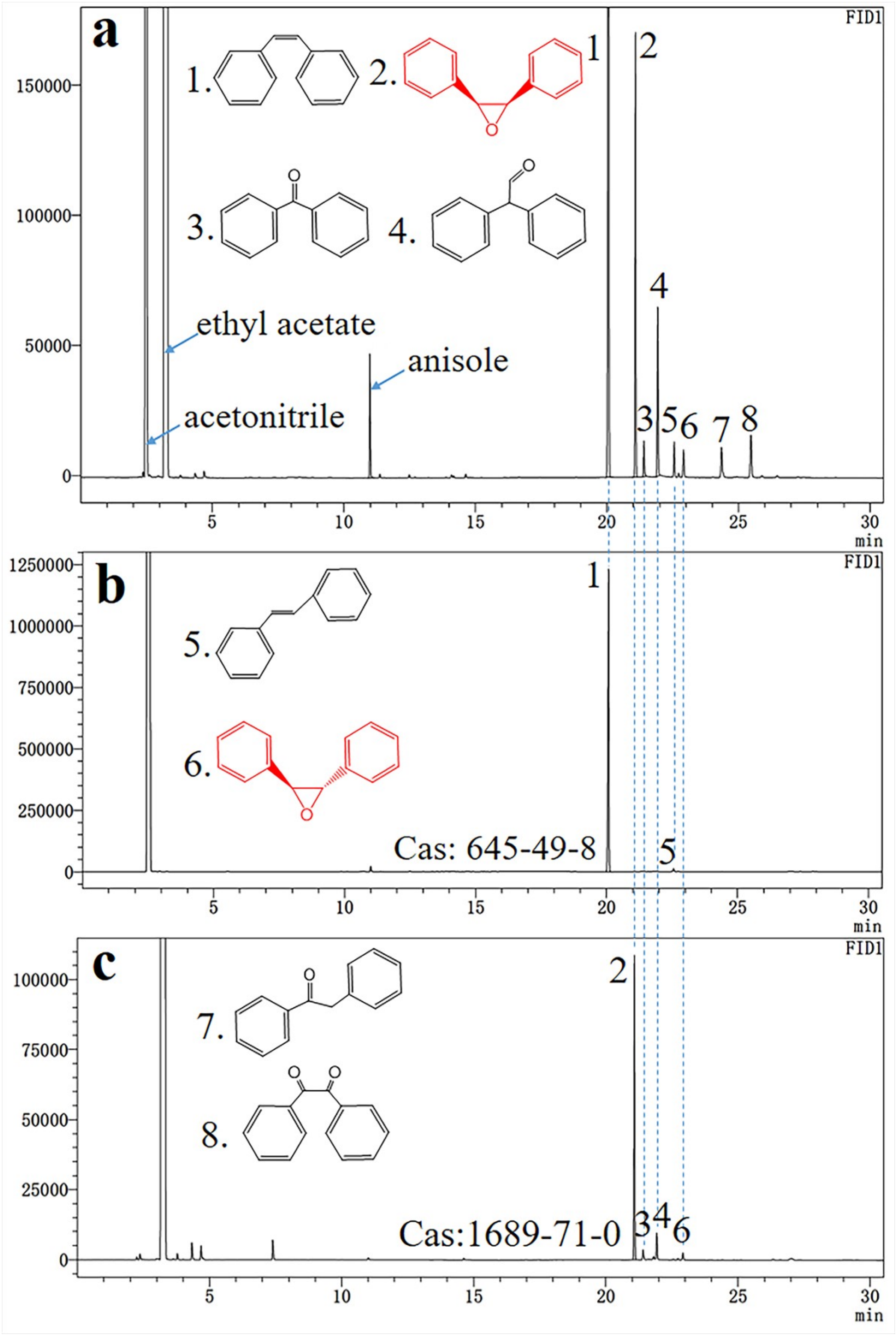

Fig. S7. The results of GC (GC-2010 PRO) chromatogram for (a) the epoxidation of cis-stilbene with H_2O_2 over $WH/WO_{2.72}$ catalyst, the reaction solvent is acetonitrile, and the extraction solvent is ethyl acetate; (b) cis-stilbene+acetonitrile, Aladdin; (c) cis-stilbene oxide+ethyl acetate, Aladdin.

Tab. S4. Comparison between catalyst used in this work and some other typical heterogeneous catalysts preciously reported in catalytic epoxidation of cyclooctene.

Entry	Catalyst	Substrate	t (h)	T (℃)	Solvent	Oxidant	Con. (%)	Sel. (%)	Ref
1	np WO_3	Cycloocten	4	80	1-butanol	H_2O_2	84	98	15
2	WO_x	Cyclooctene	2	30	CH_3CN	H_2O+O2	97	99	7
3	W-Zn/SnO_2	Cyclooctene	4	80	DMC	H_2O_2	99	99	4
4	WO_3/MCM-48	Cyclooctene	12	40	TBA	H_2O_2	99	98	16
5	WO_3-SiO_2	Cyclooctene	20	60	t-BuOH	H_2O_2	16	-	17
6	WO_3-SBA-15	Cyclooctene	3	30	CH_3CN	H_2O_2	94	100	18
7	MoO_x@HSS-2	Cyclooctene	24	80	CH_2ClCH_2Cl	H_2O_2	80	99	19
8	Nb_2O_5-SiO_2	Cyclooctene	5	70	MeOH	H_2O_2	49	100	20
9	Nb_2O_5-SiO_2(basic)	Cyclooctene	5	70	MeOH	H_2O_2	31	100	20
10	Nb_2O_5-SiO_2(acidic)	Cyclooctene	5	70	MeOH	H_2O_2	36	100	20
11	H_2WO_4/FAp	Cyclooctene	8	-	-	H_2O_2	90	-	21
12	W-MCM-41	Cyclooctene	24	-	t-BuOH	H_2O_2	98	100	22
13	**WH/$WO_{2.72}$**	**Cyclooctene**	**4**	**60**	**CH_3CN**	**H_2O_2**	**99**	**99**	**This work**

References

[1]V. T. Tran, A. K. Ravn, C. Z. Rubel, M. Xu , Y. Fu , E. M. Wagner, S. R. Wisniewski, P. Liu , W. R. Gutekunst and K. M. Engle. Ni-catalysed dicarbofunctionalization for the synthesis of sequence-encoded cyclooctene monomers. *Nat. Synth.*, 2024, **3**, 1369–1376.

[2] D. Yun, E. Z. Ayla, D. T. Bregante and D. W. Flaherty. Reactive species and reaction pathways for the oxidative cleavage of 4-octene and oleic acid with H_2O_2 over tungsten oxide catalysts. *ACS Catal.*, 2021, **11**, 3137−3152.

[3] S. Ghosh, S. S. Acharyya, T. Sasaki, and R. Bal. Fabrication of silver−tungsten wafer-like nanoarchitectures for selective epoxidation of alkenes. *ACS Sustainable Chem. Eng.*, 2015, **3**, 2823−2830.

[4] K. Kamata, K. Yonehara, Y. Sumida, K. Hirata, S. Nojima and N. Mizuno. Efficient heterogeneous epoxidation of alkenes by a supported tungsten oxide catalyst. *Angew. Chem. Int. Ed.*, 2011, **50**, 12062–12066.

[5] M. Zhang, V. Singh, X. Hu, X Ma, J. Lu, C. Zhang, J. Wang and J. Niu. Efficient olefins epoxidation on ultrafine H_2O-WO_x nanoparticles with spectroscopic evidence of intermediate species. *ACS Catal.*, 2019, **9**, 7641−7650.

[6] P. Li, J. Gao, J. Shi, H. Wang, X. Xing, J. Ren, Y. Meng, L. Wang and B. Lv. Insights into the effect of oxygen vacancies on the epoxidation of 1-hexene with hydrogen peroxide over WO_{3-x}/SBA-15. *Catal. Sci. Technol.*, 2022, **12**, 6827–6837.

[7] Y. Wang, Y. Wang, Z. Yin, X. Li, X. Gu, R. Wang and Z. Zheng. Regulation of the oxygen vacancies of WO_x for highly efficient catalytic epoxidation of cyclooctene. *Catal. Sci. Technol.*, 2025, **15**, 2008–2015.

[8] D. Hoegaerts, B. F. Sels, D. E. Vos, F. Verpoort and P. A. Jacobs. Heterogeneous tungsten-based catalysts for the epoxidation of bulky olefins. *Catal. Today*, 2000, **60**, 209–218.

[9]X. Wang, S. Wu, H Ren, P. Zhu, C. Wang, Y. Liu, S. Sun, X. Zhang, Y. Lin, Z. Meng, S. Jia and X. Han. Formation of hydroperoxo (–OOH) species on the surface of self-doped $Bi_{2.15}WO_6$: reactivity towards As(III) oxidation. *Phys. Chem. Chem. Phys.*, 2020, **22**, 12456–12464.

[10] G. Tozzola, M. A. Mantegazza, G. Ranghino, G. Petrini, S. Bordiga, G. Ricchiardi, C. Lamberti, R. Zulian and A. Zecchinay. On the structure of the active site of Ti-Silicalite in reactions with hydrogen peroxide: A vibrational and computational study. *J. Catal.*, 1988, **179**, 64–71.

[11] W. Cai, F. Chen, X. Shen, L. Chen and J. Zhang. Enhanced catalytic degradation of AO_7 in the CeO_2–H_2O_2 system with Fe^{3+} doping. *Appl. Catal. B*, 2010, **101**, 160–168.

[12] P. Wang, S. Guo, Z. Hu, T. Li, S. Pu, H. Mao, H. Cai, Z. Zhu, H. Li and H. Liu. $W_{18}O_{49}$ sensitized with Pd nanoparticles for ultrasensitive ppb-level formaldehyde detection. *Chem. Eng. J.*, 2023, **456**, 140988.

[13] Y. Nakagawa and N. Mizuno. Mechanism of $[\gamma\text{-}H_2SiV_2W_{10}O_{40}]^{4-}$-catalyzed epoxidation of alkenes with hydrogen peroxide. *Inorg. Chem.*, 2007, **46**, 1727−1736.

[14] Z. Xie, L. Gao, B. Liang, X. Wang, G. Chen, Z. Liu, J. Chao, D. Chen and G. Shen. Fast fabrication of a $WO_3 \cdot 2H_2O$ thin film with improved electrochromic properties. *J. Mater. Chem.*, 2012, **22**, 19904–19910.

[15] C. Hammond, J. Straus, M. Righettoni, S. E. Pratsinis and I. Hermans. Nanoparticulate tungsten oxide for catalytic epoxidations. *ACS Catal.*, 2013, **3**, 321–327.

[16] D. H. Koo, M. Kim and S. Chang. WO_3 nanoparticles on MCM-48 as a highly selective and versatile heterogeneous catalyst for the oxidation of olefins, sulfides, and cyclic ketones. *Org. Lett.*, 2005, **7**, 5015–5018.

[17] R. Neumann, M. Chava and M. Levin. Hydrogen peroxide oxidations catalysed by metallosilicalite xerogels. *J. Chem. Soc.*, *Chem. Commun.*, 1993, **22**, 1685–1687.

[18] Y. Kuwahara, N. Furuichi, H. Seki and H. Yamashita. One-pot synthesis of molybdenum oxide nanoparticles encapsulated in hollow silica spheres: an efficient and reusable catalyst for epoxidation of olefins. *J. Mater. Chem. A*, 2017, **5**, 18518–18526.

[19] F. Somma, A. Puppinato and G. Strukul. Niobia‐silica aerogel mixed oxide catalysts: effects of the niobium content, the calcination temperature and the surface hydrophilicity on the epoxidation of olefins with hydrogen peroxide. *Appl. Catal., A*, 2006, **309**, 115–121.

[20］ F. Somma, P. Canton and G. Strukul. Effect of the matrix in niobium-based aerogel catalysts for the selective oxidation of olefins with hydrogen peroxide. *J. Catal.*, 2005, **229**, 490–498.

[21] J. Ichihara. Solvent-free epoxidation using a tungstic acid catalyst on fluoroapatite. *Tetrahedron Lett.*, 2001, **42**, 695–697.

[22] J. M. Brégeault, J. Y. Piquemal, E. Briot, E. Duprey and A. P. Legrand. New approaches to anchoring or inserting highly dispersed tungsten oxo(peroxo) species in mesoporous silicates. *Microporous Mesoporous Mater.*, 2001, **44**, 409–417.